

CoMFA, Molecular Docking and Molecular Dynamics Studies on Cycloguanil Analogues as Potent Antimalarial Agents

Isman Kurniawan^{1,*}, Muhamad Salman Fareza², and Ponco Iswanto³

¹School of Computing, Telkom University, Jl. Telekomunikasi, Terusan Buah Batu, Bandung 40257, Indonesia

²Department of Pharmacy, Universitas Jenderal Soedirman, Jl. Dr. Soeparno, Karangwangkal, Purwokerto 53123, Indonesia

³Department of Chemistry, Universitas Jenderal Soedirman, Jl. Dr. Soeparno, Karangwangkal, Purwokerto 53123, Indonesia

* **Corresponding author:**

email: ismankrn@telkomuniversity.ac.id

Received: December 10, 2019

Accepted: April 3, 2020

DOI: 10.22146/ijc.52388

Abstract: Malaria is a disease that commonly infects humans in many tropical areas. This disease becomes a serious problem because of the high resistance of *Plasmodium* parasite against the well-established antimalarial agents, such as Artemisinin. Hence, new potent compounds are urgently needed to resolve this resistance problem. In the present study, we investigated cycloguanil analogues as a potent antimalarial agent by utilizing several studies, i.e., comparative of molecular field analysis (CoMFA), molecular docking and molecular dynamics (MD) simulation. A CoMFA model with five partial least square regressions (PLSR) was developed to predict the pIC₅₀ value of the compound by utilizing a data set of 42 cycloguanil analogues. From statistical analysis, we obtained the r^2 values of the training and test sets that were 0.85 and 0.70, respectively, while q^2 of the leave-one-out cross-validation was 0.77. The contour maps of the CoMFA model were also interpreted to analyze the structural requirement regarding electrostatic and steric factors. The most active compound (c33) and least active compound (c8) were picked for molecular docking and MD analysis. From the docking analysis, we found that the attached substituent on the backbone structure of cycloguanil gives a significant contribution to antimalarial activity. The results of the MD simulation confirm the stability of the binding pose obtained from the docking simulations.

Keywords: malaria; cycloguanil; CoMFA; molecular docking; molecular dynamics

■ INTRODUCTION

Malaria is a life-threatening disease that causes public health problems in many regions of Africa and Asia. In 2016, malaria had infected 216 million people across the world and had caused 445,000 deaths, as reported by the World Health Organization [1]. Furthermore, this disease leads to the increase of economic and social burden on infected patients [2]. This disease is mostly caused by the *Plasmodium falciparum* parasite which is a major factor of malaria-related deaths in the world. Several antimalarial drugs, such as chloroquine, pyrimethamine, and cycloguanil, have been used to treat the infection of malaria. These drugs act as antimalarial agents by inhibiting the activity of dihydrofolate reductase of *P. falciparum* enzyme, i.e., dihydrofolate reductase-

thymidylate synthase (PfDHFR-TS) [3].

However, the resistance of the parasite against well-established antimalarial agents has been found in many countries. The widespread occurrences of malaria could be the main factor of this resistance [4]. Therefore, new antimalarial drugs are urgently required to overcome the resistance problem. Regarding this issue, a series of cycloguanil analogues which are known to have an ability to effectively bind to wild type and mutant type PfDHFR, an antimalarial drug target, have been employed in this study [5-6]. The cycloguanil analogues backbone contains 1,3,5-dihydrotriazine in which *p*-chlorophenyl is attached at N1 position, as shown in Fig. 1.

In silico approach is commonly used to design the new drug candidate by investigating the type of attached

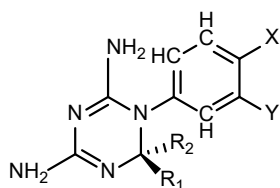


Fig 1. Chemical structure of cycloguanil analogues

substituent in cycloguanil analogues. Several studies have been reported concerning the utilization of *in silico* approaches, such as quantitative structure-activity relationship (QSAR) [7-8], pharmacophore [9], homology modelling [10], molecular docking [9], and molecular dynamics [11], in designing new drug candidates. Relating to *in silico* studies on cycloguanil analogues as an antimalarial agent, Kuhmar Ojha and co-workers have performed QSAR, pharmacophore mapping and docking studies to obtain cycloguanil derivatives with high binding affinity against PfDHFR-TS target [12]. A prediction model of cycloguanil analogues has also been developed by Nattee and co-workers. They used an extremely randomized tree to develop the model and obtained a satisfying result [13]. In addition, Inthajak and co-workers developed a QSAR model to predict the activity of cycloguanil analogues by using PSO-SVR method [14]. However, to the best of our knowledge, there is no report on the investigation of the dynamics of cycloguanil analogues and the DHFR receptor.

In this study, we utilized a series of *in silico* approach, i.e., comparative of molecular field analysis (CoMFA), molecular docking, and molecular dynamics, to explore the structural contribution of cycloguanil analogues on antimalarial activity. The observed pIC_{50} values were considered as target values in developing the CoMFA model. The contribution of a steric and electrostatic factor was revealed by carrying out contour maps analysis. We also investigated the binding pose of the complex of cycloguanil analogues and the receptor target by using molecular docking. Finally, the binding pose was confirmed by carrying out molecular dynamic simulation.

■ COMPUTATIONAL METHODS

Molecular Data Set

A series of 42 cycloguanil analogues, used in this

study, were obtained from references [6,15]. The experimental IC_{50} values of the compounds at nano-molar (nM) units were converted to molar (M) units. To obtain target values in a smaller range, we converted the IC_{50} to pIC_{50} by using the formula $pIC_{50} = -\log IC_{50}$. Then, pIC_{50} values were used as target values for the development of the CoMFA model. From the data set, training and test sets which contain 32 and 10 compounds, respectively, were randomly selected. The chemical structure and experimental pIC_{50} values of cycloguanil analogues are provided in Table 1. The 2D structures of the compounds were constructed by using the MarvinSketch program [16] and were converted to a 3D structure by using Open Babel package [17]. The structures were optimized by using AM1 method in MOPAC package [18] and were converted to SDF file format containing all compound structures. This SDF file was used for performing molecular alignment of CoMFA analysis.

CoMFA Modelling

The CoMFA model was developed by utilizing the optimized compound structure with pIC_{50} as the target values. The development of the CoMFA model was begun by performing molecular alignment analysis by using Open3DALIGN package [19]. In this stage, molecular alignment processes were performed by using each compound as a template, so 42 alignments were generated. The alignment with compound 42 (c42) as a template, as shown in Fig. 2, has the maximum alignment score and thus was considered for developing the CoMFA model.

CoMFA model was built in Open3DQSAR package [20] by inserting the alignment with c42 as a template into a grid box with 1 Å grid spacing and was expanded to 5 Å in all directions from the alignment as the center. Molecular interaction fields (MIF) were generated in terms of the steric field and electrostatic field. For the steric field, MIF was calculated by using a carbon atom probe, while for the electrostatic field, MIF was calculated by using a volume-less probe with +1 charge. Before building the model, pre-treatment processes were performed to obtain an acceptable

model. The pre-treatment processes consisted of the following steps: (a) determination of the cut-off of maximum and minimum energy values at ± 30 kcal/mol, (b) interaction fields with the values of absolute energy lower than 0.05 were adjusted to zero, (c) independent variables with the value of standard deviation lower than 0.1 were removed, (d) independent variables matrices were scaled with the block unscaled weighting (BUW) technique [20-21].

To increase the interpretability, a variable selection procedure was carried out to discard fewer influent variables. This procedure was performed by using the combination of smart region definition (SRD) and factorial design (FFD) [20,22]. Ten cycloguanil analogues

data were randomly selected for a test set, while the rest of the data was set as a training set. Finally, a prediction model was built with partial least square regression (PLSR) by utilizing the pIC_{50} values as the dependent

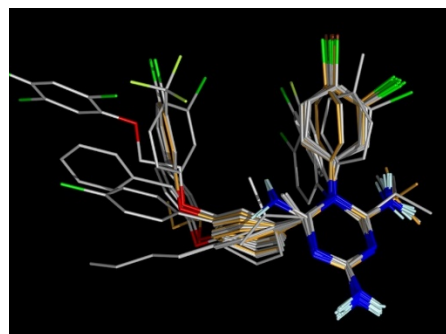
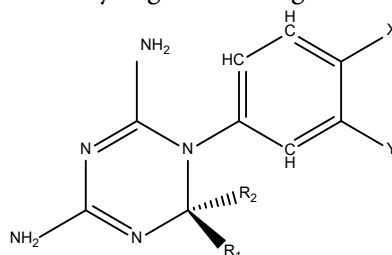


Fig 2. The best alignment with c42 as a template

Table 1. Data set of cycloguanil analogues used in this study



Comp.	R1	R2	X	Y	pIC_{50}	Comp.	R1	R2	X	Y	pIC_{50}
1	CH ₃	CH ₃	Cl	H	5.61	22	CH ₃	CH ₃	H	H	6.35
2	H	H	Cl	H	6.50	23 ^a	CH ₃	CH ₃	F	H	6.00
3	CH ₃	H	Cl	H	6.46	24	H	H	H	H	6.45
4 ^a	CH ₂ CH ₃	H	Cl	H	6.31	25	H	H	F	H	6.51
5	(CH ₂) ₂ CH ₃	H	Cl	H	6.64	26	CH ₃	CH ₃	H	Cl	6.53
6	(CH ₂) ₃ CH ₃	H	Cl	H	6.60	27	CH ₃	CH ₃	Cl	Cl	6.51
7 ^a	CH(CH ₃) ₂	H	Cl	H	5.55	28 ^a	CH ₃	H	H	Cl	7.55
8	C(CH ₃) ₃	H	Cl	H	4.18	29	CH ₃	H	Cl	Cl	7.72
9	C ₆ H ₅	CH ₃	Cl	H	7.36	30 ^a	C ₆ H ₅	H	H	Cl	7.62
10	CH ₃	CH ₃	Br	H	5.56	31	C ₆ H ₅	H	Cl	Cl	7.54
11	CH ₃	H	Br	H	6.56	32	C ₆ H ₄ -p-OC ₆ H ₅	H	Cl	H	7.40
12 ^a	CH ₂ CH ₃	H	Br	H	6.66	33	C ₆ H ₄ -p-OC ₆ H ₅	H	H	Cl	8.40
13	(CH ₂) ₂ CH ₃	H	Br	H	6.60	34 ^a	C ₆ H ₄ -m-OC ₆ H ₅	H	H	Cl	7.22
14	CH(CH ₃) ₂	H	Br	H	6.14	35	C ₆ H ₄ -m-OCH ₂ C ₆ H ₅	H	H	Cl	6.72
15 ^a	C ₆ H ₅	H	Br	H	6.74	36	C ₆ H ₄ -m-(OC ₆ H ₄ -4-Cl)	H	Cl	H	6.38
16	CH ₃	CH ₃	CH ₃	H	5.44	37	C ₆ H ₄ -m-(4-ClC ₆ H ₄)	H	H	Cl	6.41
17	CH ₃	H	CH ₃	H	6.33	38	n-C ₇ H ₁₅	H	H	Cl	8.40
18 ^a	CH ₂ CH ₃	H	CH ₃	H	6.29	39 ^a	C ₆ H ₄ -p-OC ₃ H ₇	H	H	Cl	8.40
19	(CH ₂) ₂ CH ₃	H	CH ₃	H	6.82	40	C ₆ H ₄ -m-(OC ₆ H ₃ -3,5-Cl ₂)	H	H	Cl	7.30
20	CH(CH ₃) ₂	H	CH ₃	H	5.46	41	C ₆ H ₄ -m-O(CH ₂) ₂ -O(2,4,5-Cl ₃ -C ₆ H ₂)	H	H	Cl	6.43
21	C ₆ H ₅	H	CH ₃	H	7.41	42	C ₆ H ₄ -m-(3-CF ₃ -OC ₆ H ₄)	H	H	Cl	6.74

^a refers test set compound

variables and selected CoMFA variables as independent variables.

Model Validation

To validate the CoMFA model, we performed both internal and external validation tests and compared the value with the threshold. The internal validation was performed by calculating the coefficient of determination (R_{train}^2) and leave-one-out (LOO) cross-validation (Q_{loo}^2) using the training set. Meanwhile, the external validation was conducted by calculating the coefficient of determination (R_{test}^2) using the test set. The model was acceptable if the value of R^2 and Q^2 were more than 0.6 and 0.5, respectively. Furthermore, several validation parameters were calculated to confirm the acceptability of the model. The calculation of the validation parameters is summarized as follows

$$R_{\text{train}}^2 = 1 - \frac{\sum(y_{\text{train}} - \hat{y}_{\text{train}})^2}{\sum(y_{\text{train}} - \bar{y}_{\text{train}})^2} \quad (1)$$

$$Q_{\text{loo}}^2 = 1 - \frac{\sum(y_{\text{train}} - \hat{y}_{\text{loo}})^2}{\sum(y_{\text{train}} - \bar{y}_{\text{train}})^2} \quad (2)$$

$$R_{\text{test}}^2 = 1 - \frac{\sum(y_{\text{test}} - \hat{y}_{\text{test}})^2}{\sum(y_{\text{test}} - \bar{y}_{\text{train}})^2} \quad (3)$$

$$k = \frac{\sum(y \times \hat{y})}{\sum(\hat{y})^2} \quad (4)$$

$$k' = \frac{\sum(y \times \hat{y})}{\sum(y)^2} \quad (5)$$

$$r^2 = \frac{[\sum(y - \bar{y})(\hat{y} - \bar{\hat{y}})]^2}{\sum(y - \bar{y})^2 \times \sum(\hat{y} - \bar{\hat{y}})^2} \quad (6)$$

$$r_0^2 = 1 - \frac{\sum(y - k \times \hat{y})^2}{\sum(y - \bar{y})^2} \quad (7)$$

$$r_0'^2 = 1 - \frac{\sum(\hat{y} - k' \times y)^2}{\sum(\hat{y} - \bar{\hat{y}})^2} \quad (8)$$

$$r_m^2 = r^2 \times \left(1 - \sqrt{r^2 - r_0^2}\right) \quad (9)$$

$$r_m'^2 = r^2 \times \left(1 - \sqrt{r^2 - r_0'^2}\right) \quad (10)$$

$$\bar{r}_m^2 = \frac{(r_m^2 + r_m'^2)}{2} \quad (11)$$

$$\Delta r_m^2 = |r_m^2 - r_m'^2| \quad (12)$$

$${}^c R_p^2 = R \times \sqrt{R^2 - R_r^2} \quad (13)$$

where y and \hat{y} represent the experimental and predicted value of pIC_{50} , respectively, while \bar{y} and $\bar{\hat{y}}$ represent the average of the experimental and predicted value, respectively. The value of ${}^c R_p^2$ represents the correlation coefficient which is calculated by considering randomized and non-randomized models. This parameter can be used to verify that the model is not overfitting. The acceptability of the model was considered according to the following criteria [23-25]

$$R^2 > 0.6$$

$$Q^2 > 0.5$$

$$0.85 \leq k \leq 1.15 \text{ or } 0.85 \leq k' \leq 1.15$$

$$\frac{(r^2 - r_0^2)}{r^2} < 0.1 \text{ or } \frac{(r^2 - r_0'^2)}{r^2} < 0.1$$

$$|r_0^2 - r_0'^2| < 0.3$$

$$\bar{r}_m^2 > 0.5$$

$$\Delta r_m^2 < 0.2$$

$${}^c R_p^2 > 0.5$$

Applicability domain (AD) of the model was also determined to confirm that the data set lies in the domain of the model. The determination of AD was performed by using leverage method that is formulated as $H = X(X^T X)^{-1} X^T$ (14) where X represents the score matrix obtained from the PLSR procedure. The critical leverage (h^*) value was defined as $3p/n$, where p and n are the numbers of attributes and data set, respectively, that are involved in the training process. The predicted value of a data set was acceptable if the calculated leverage value was smaller than the critical leverage. The AD of the CoMFA model was figured out by using the William plot [26]. Finally, we interpreted the CoMFA contour map of the steric and electrostatic factors by using MacPymol package [27].

Molecular Docking

According to the pIC_{50} values, the most active (c33) and least active compound (c8) were selected for further

analysis of molecular docking and molecular dynamics simulation. Regarding the docking scenario, we implemented a flexible ligand-rigid receptor scheme to represent lock and key theory of ligand-receptor interaction. The receptor molecule was prepared by downloading the X-ray crystal structure of wild-type *Plasmodium falciparum* DHFR-TS complexed with cycloguanil and NADPH at 2.6 Å resolution (PDB ID: 3UM8, <https://www.rcsb.org/structure/3um8>) from RCSB protein data bank [28]. The binding site of the receptor was identified from the position of native cycloguanil found in the X-ray structure. However, we removed the original cycloguanil from the structure as part of the preparation process.

To construct pdbqt file of the receptor, we used Open Babel package [17] to add polar hydrogens and assign Gasteier charge to the ligand. The grid box, which defines the docking area, was constructed by using the native ligand position as the center and expanded the box with a size of 8 Å. The docking simulation was performed by using Smina docking package [29] and the binding pose obtained from the docking simulation was plotted by using LigPlot package [30].

The docking procedure was validated by extracting native cycloguanil ligand from wild-type *Plasmodium falciparum* DHFR-TS complex and re-docking the ligand to the receptor. The validity of the method was determined by aligning the ligand obtained from docking simulation and original X-ray crystal structure, and calculating the deviation between both structures. In this case, the deviation was represented as the root mean square displacement (RMSD) parameter.

Molecular Dynamics

The binding poses of the docked ligand into the receptor were obtained instantaneously from docking simulation. Consequently, the interaction may be unstable due to the rigid receptor approximation. Therefore, we confirmed the stability and validity of the interaction by carrying out molecular dynamics simulation for the complex system. The molecular dynamics simulation of ligand-protein complexes was performed by using Gromacs 2018 package [31].

The preparation of the structure of the complex was carried out by using MacPymol package [27]. The topology of protein was prepared by using CHARMM36 force field. Meanwhile, the topology of ligand was estimated by using CHARMM General Force Field (CGenFF) server (<https://cgenff.umaryland.edu/>). Then, the complex was solvated into dodecahedron box of SPC water with 1.00 nm from the molecule to the edge of the box. The solvated complex system was neutralized by replacing the solvent molecule with Cl⁻ ions.

After completing the preparation step, the system was minimized by using the steepest descent algorithm, followed by consecutive NVT (1 ns) and NPT (1 ns) equilibrations. During the equilibrations, the temperature was fixed at 300 K by utilizing V-rescale thermostat algorithm [32], and the pressure was fixed at 1.0 bar by utilizing Berendsen barostat algorithm [33]. Finally, MD simulation was performed for 20 ns with a time step of 2 fs. Neighbor searching was carried out by using Verlet algorithm with a cut-off radius of Van der Waals (VdW) short interaction that was set at 1.2 nm. Long-range electrostatic interaction was carried out by using Particle Mesh Ewald scheme-38 with a cut-off radius set at 1.2 nm. The results of the simulation were investigated by using Gromacs analysis tools [31].

RESULTS AND DISCUSSION

CoMFA Modelling

To develop the CoMFA model, we used the best alignment of molecules by considering the c42 molecule as a template. The model was developed by using the partial least square regressions (PLSR) method with five PLS components. The comparison of predicted and experimental values of pIC₅₀ is shown in Fig. 3(a), while the Williams plot that represents the applicability domain (AD) of the model is shown in Fig. 3(b). Those analyses confirm that all of the data lie inside the AD region, indicating that no outlier data existed in the data set. Furthermore, the predictive model is confirmed to be acceptable for all compounds. To validate the CoMFA model, several statistical parameters were calculated and compared to threshold values [23-25]. We found that the calculated values of the validation parameters, as provided

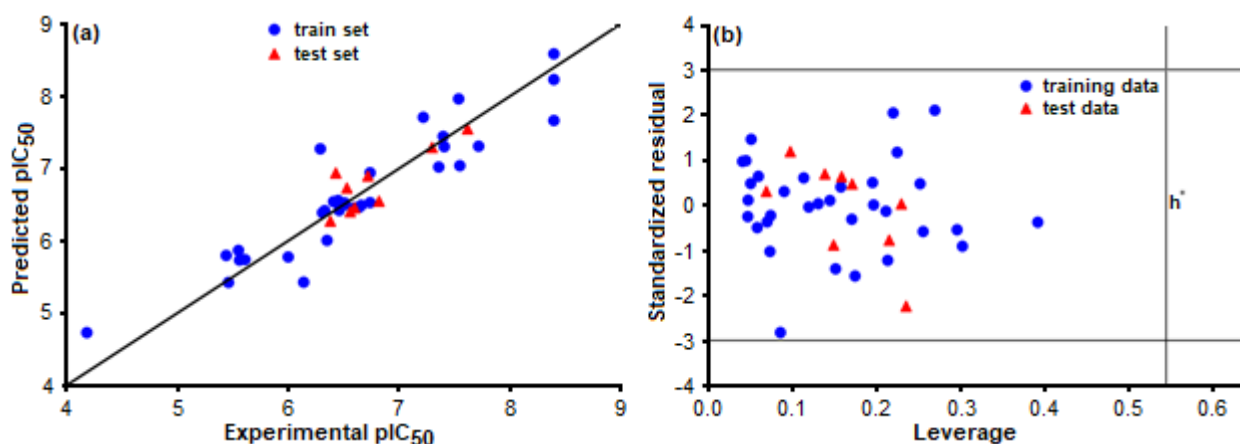


Fig 3. (a) Scatter plot of predicted pIC_{50} vs. experimental pIC_{50} ; (b) Williams plot of applicability domain

in Table 2, met the criteria. These results indicate that the CoMFA model was valid and acceptable. In addition, we found that the value of ${}^cR_p^2$ is larger than 0.5, which indicates that the model is not overfitting.

The contour maps of the CoMFA model that represent the steric and electrostatic field of favorable substituents are presented in Fig. 4. In the steric field, the green and yellow contours depict the favorable and unfavorable position, respectively, for bulky group substituents. Meanwhile, in the electrostatic field, the red and blue contours depict the favorable position for negatively and positively charged substituents, respectively. In the steric contour map, we found a large green contour around R_1 position. This indicates that bulky

Table 2. Calculated statistical parameter of CoMFA model

Parameter	Training set	Test set	Threshold [23-25]
R^2	0.85	0.70	> 0.6
Q^2	0.77	-	> 0.5
k'	0.86	1.05	$0.85 \leq k' \leq 1.15$
$\frac{(r^2 - r_0^2)}{r^2}$	0.07	0.00	< 0.1
$\left \frac{r_0^2 - r_0'^2}{r_0^2} \right $	0.05	0.09	< 0.3
$\overline{r_m^2}$	0.72	0.57	> 0.5
$\Delta \overline{r_m^2}$	0.14	0.18	< 0.2
${}^cR_p^2$	0.76	-	> 0.5

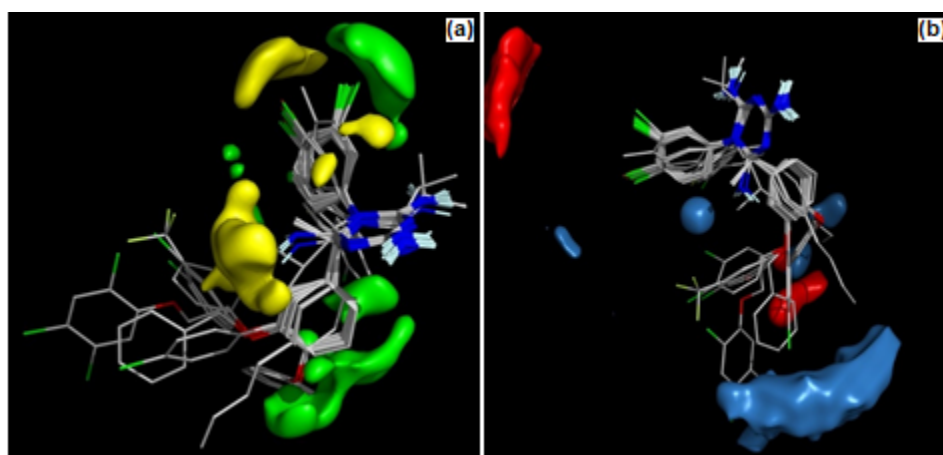


Fig 4. (a) Steric CoMFA contour map, green and yellow contour indicate a region where bulky substituent is favorable and unfavorable, respectively; (b) Electrostatic CoMFA contour map, red and blue contour indicate a favorable region for a substituent with positively and negatively charged, respectively

group substituents are favorable to attach at this position. Among the data set, several compounds contained a bulky group attached at R_1 position, namely c9, c15, c21, c32–c42. The greater activity of c9 compared to c1 corresponds to the substitution of the methyl group of c1 by the phenyl group of c9. Therefore, the attachment of a phenyl group at R_1 position increased the steric effect and thus increased the activity of the compounds.

Besides that, the green contour was also found around the X position that indicates a favorable position for the more steric group at this position. The greater activity of c12 compared to c4 was also related to the increase of the steric effect of the substituent at this position, namely Br^- and Cl^- for c12 and c4, respectively. Meanwhile, the yellow contours were found around the R_2 position that indicates the unfavorable position for a bulky group in this position. We found that most of the compounds in the data set had a low steric substituent. The attachment of more steric substituents at this position decreased the activity of the compound. This finding was confirmed by the comparison of the pIC_{50} of c1 (5.61) with a methyl substituent that was greater than c3 (6.46) with a hydrogen substituent. In addition, yellow contours were found around the Y position that indicates the unfavorable position for a bulky group in this position.

In the electrostatic contours, we found two dominant contours that consists of one blue contour around the R_1 position and one red contour around the X and Y positions. This indicates that positively charged substituents are favorable to attach at R_1 position, while negatively charged substituents are favorable to attach to both X and Y position. The activity of c4 was higher than that of c5 due to the existence of a more positive (ethyl group) substituent. Generally, the increase in the activity of a molecule was related to the increase in the negative charge of the substituent at X and Y positions. For example, the attachment of Cl^- substituent at c26 contributed to the higher activity of the molecule compared to that of c22.

Molecular Docking

Molecular docking analysis was carried out on the most active compound (c33) and the least active

compound (c8). We found that the calculated binding score for c33 and c8 compound were -10.7 kcal/mol and -7.9 kcal/mol, respectively. The lower value of the binding score indicated that c33 binds to the receptor better than c8, which is in agreement with the experimental results. The binding poses of both compounds that were docked into 3UM8 receptor, obtained from the docking simulation, are provided in Fig. 5(a) and 5(b). From the binding poses, we found that both compounds were docked in a similar binding site of the receptor.

The 2D plots of ligand-receptor interaction between c33 and c8 compounds with 3UM8 receptor are presented in Fig. 5(c) and 5(d). The number of hydrogen bonds found in the interaction of the receptor with c33 and c8 were four and one, respectively. For c33 ligands, the hydrogen bonds were found in the interaction of the ligands with ALA16, LEU40 and SER111. Meanwhile for c8 ligands, a hydrogen bond was found in the interaction of the ligands with ALA16. From the docking results, we found that the higher number of hydrogen bonds found in c33-receptor interaction contributed to the high activity of the ligand.

The acceptability of our docking simulations was confirmed by validating the docking procedure. The validity of the procedure was represented by the value of RMSD of the alignment between the ligand configuration obtained from docking simulation and the original X-ray crystal structure, in which the alignment is shown in Fig. 6. According to the validation analysis, we found that the RMSD value is 1.09 Å, which is low enough to confirm that the docking procedure is valid [34].

Molecular Dynamics

To confirm the stability of the solvated complex system, we analyzed the fluctuation of RMSD and the radius of gyration for 20 ns simulation of both complexes, as shown in Fig. 7(a). RMSD analysis shows that both c33 and c8 complexes reached the equilibrium state after 10 ns. We also found that the RMSD value of the c33 complex was slightly lower than that of the c8 complex, indicating the better stability of the c33 complex. The fluctuation of the radius of gyration, which

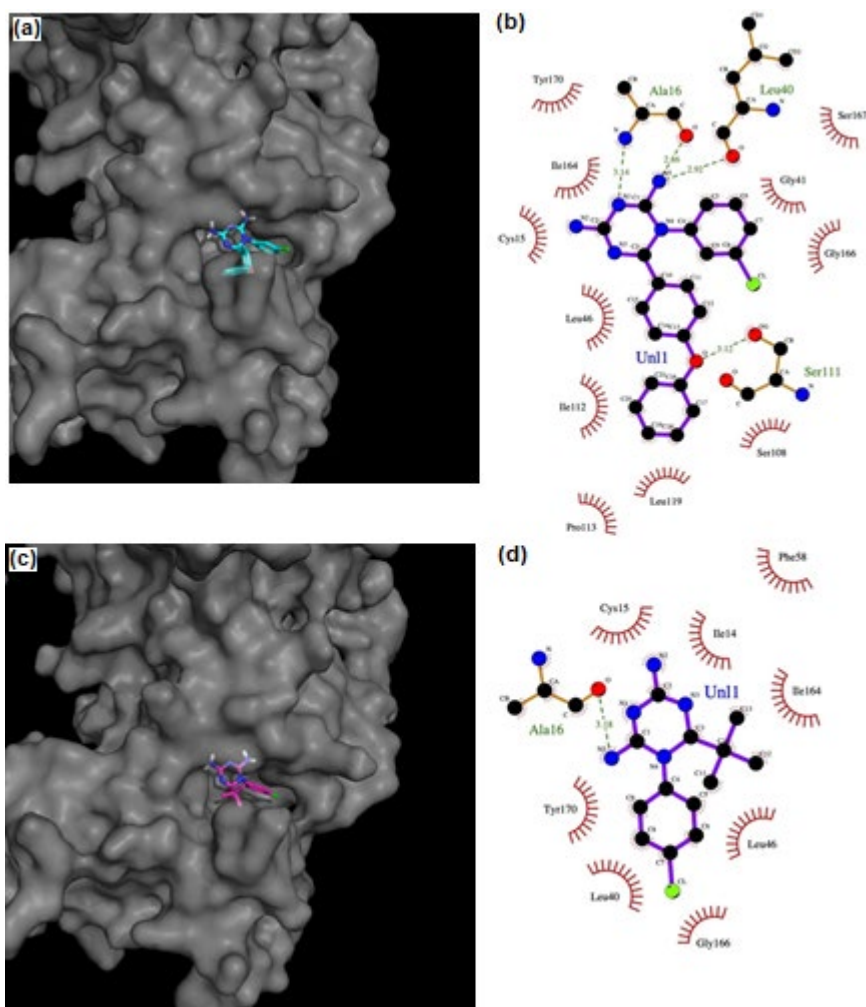


Fig 5. The binding poses of (a) c33 and (c) c8 that are docked into 3UM8 binding site, and the plot of ligand-receptor interaction of (b) c33 and (d) c8 ligands

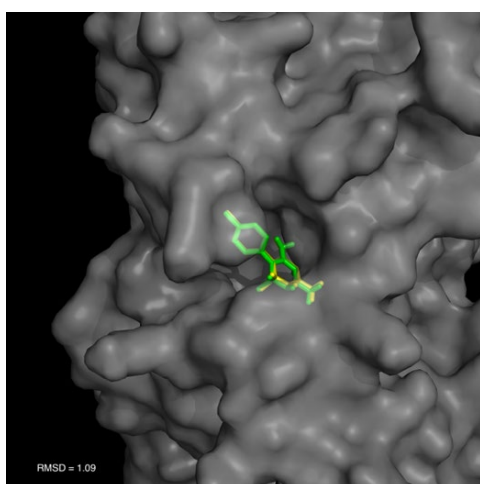


Fig 6. The alignment of the ligand configuration obtained from docking simulation (green) and original X-ray crystal structure (yellow)

indicates the compactness of the complex system, is provided in Fig. 7(b). We found that the compactness of the c33 complex was lower than that of the c8 complex.

We also analyzed the fluctuation of the hydrogen bond formed during the simulation, as shown in Fig. 7(c). We found that the hydrogen bond formed during the simulation of the c33 complex was more than that of the c8 complex. In the case of the c33 complex, the maximum number and the average number of hydrogen bonds were 4 and 0.78, respectively. Meanwhile, in the case of the c8 complex, the maximum number and the average number of hydrogen bonds were 3 and 0.82, respectively. According to the results, it seems that the number of hydrogen bonds formed during the simulation was quite similar between both complexes.

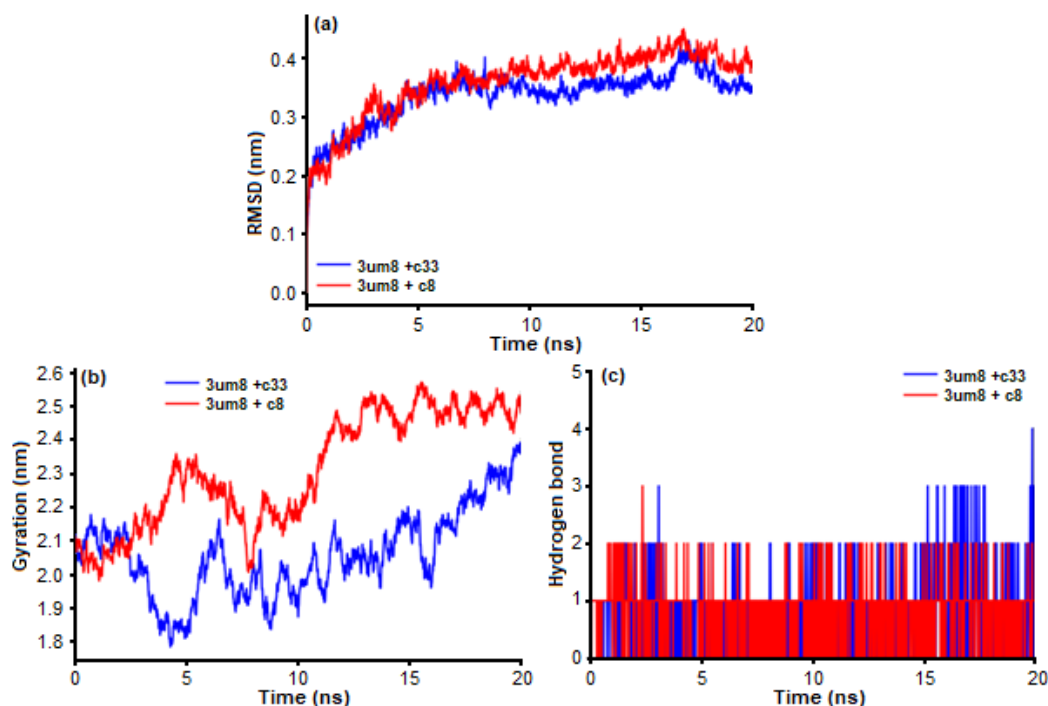


Fig 7. Plots of (a) RMSD, (b) radius of gyration and (c) hydrogen bonds number from MD simulation of c33 and c8 complex

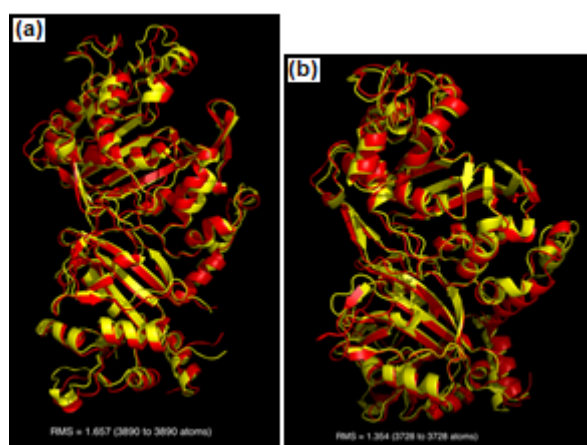


Fig 8. The alignment of the initial (yellow) and final (red) structure obtained from MD simulation of 3UM8 complex with (a) c33 and (b) c8 ligand

Finally, we aligned the final structure of the complex obtained from MD simulation with the initial structure to verify that the structure did not change significantly during the simulation. The results of the alignment for both complexes are presented in Fig. 8. We found that the final structure for both complexes resembles the initial structure with a small deviation. This is indicated by the low RMSD that is evaluated from the alignment processes, which

were 1.657 Å and 1.354 Å for the complex with c33 and c8, respectively. This points out that the structure did not change significantly during the simulation.

■ CONCLUSION

This study aims to explore the structural contribution of cycloguanil analogues on antimalarial activity. The CoMFA model was developed and validated by using several statistical parameters. Based on contour maps analysis, the bulky group with a positively charged atom was favorable to attach at the R1 position, while the bulky group with a negatively charged atom was favorable to attach at the Y position. From the docking analysis, we found that the existing hydrogen bonds in the binding pose of c33 was more than that of c8. This finding points out the importance of the hydrogen bond in supporting inhibition activity. The results of the MD simulation confirmed the stability of the binding pose obtained from the docking simulation.

■ ACKNOWLEDGMENTS

This work was supported in part through High Performance Computing (HPC) resources provided by

the School of Computing, Telkom University.

■ REFERENCES

- [1] World Health Organization, 2018, *Ready to beat malaria*, World Malaria Day 2018, 26 March 2018, 1–3.
- [2] Alonso, S., Chaccour, C.J., Elobolobo, E., Nacima, A., Candrinho, B., Saifodine, A., Saute, F., Robertson, M., and Zulliger, R., 2019, The economic burden of malaria on households and the health system in a high transmission district of Mozambique, *Malar. J.*, 18 (1), 360.
- [3] Mharakurwa, S., Kumwenda, T., Mkulama, M.A.P., Musapa, M., Chishimba, S., Shiff, C.J., Sullivan, D.J., Thuma, P.E., Liu, K., and Agre, P., 2011, Malaria antifolate resistance with contrasting *Plasmodium falciparum* dihydrofolate reductase (DHFR) polymorphisms in humans and *Anopheles* mosquitoes, *Proc. Natl. Acad. Sci. U.S.A.*, 108 (46), 18796–18801.
- [4] Blasco, B., Leroy, D., and Fidock, D.A., 2017, Antimalarial drug resistance: Linking *Plasmodium falciparum* parasite biology to the clinic, *Nat. Med.*, 23 (8), 917–928.
- [5] Yuthavong, Y., Tarnchompoo, B., Vilaivan, T., Chitnumsub, P., Kamchonwongpaisan, S., Charman, S.A., McLennan, D.N., White, K.L., Vivas, L., Bongard, E., Thongphanchang, C., Tawechai, S., Vanichtanankul, J., Rattanajak, R., Arwon, U., Fantauzzi, P., Yuvaniyama, J., Charman, W.N., and Matthews, D., 2012, Malarial dihydrofolate reductase as a paradigm for drug development against a resistance-compromised target, *Proc. Natl. Acad. Sci. U.S.A.*, 109 (42), 16823–16828.
- [6] Kulatee, S., Toochinda, P., Suksangpanomrung, A., and Lawtrakul, L., 2017, Theoretical investigation of the enantioselective complexations between *pf*DHFR and cycloguanil derivatives, *Sci. Pharm.*, 85 (4), 37.
- [7] Kurniawan, I., Rosalinda, M., and Ikhsan, N., 2020, Implementation of ensemble methods on QSAR Study of NS3 inhibitor activity as anti-dengue agent, *SAR QSAR Environ. Res.*, 31 (6), 477–492.
- [8] Kurniawan, I., Tarwidi, D., and Jondri, 2019, QSAR modeling of PTP1B inhibitor by using Genetic algorithm-Neural network methods, *J. Phys. Conf. Ser.*, 1192, 012059.
- [9] Sattarov, B., Baskin, I.I., Horvath, D., Marcou, G., Bjerrum, E.J., and Varnek, A., 2019, De novo molecular design by combining deep autoencoder recurrent neural networks with generative topographic mapping, *J. Chem. Inf. Model.*, 59 (3), 1182–1196.
- [10] Hu, X., Xie, J., Hu, S., Zhang, L., and Dong, Y., 2017, Exploration of the binding affinities between ecdysone agonists and EcR/USP by docking and MM-PB/GBSA approaches, *J. Mol. Model.*, 23 (5), 166.
- [11] Dehury, B., Behera, S.K., and Mahapatra, N., 2017, Structural dynamics of Casein Kinase I (CKI) from malarial parasite *Plasmodium falciparum* (Isolate 3D7): Insights from theoretical modelling and molecular simulations, *J. Mol. Graphics Modell.*, 71, 154–166.
- [12] Ojha, P.K., and Roy, K., 2011, Exploring QSAR, pharmacophore mapping and docking studies and virtual library generation for cycloguanil derivatives as PfDHFR-TS inhibitors, *Med. Chem.*, 7 (3), 173–199.
- [13] Nattee, C., Khamsemanan, N., Lawtrakul, L., Toochinda, P., and Hannongbua, S., 2017, A novel prediction approach for antimalarial activities of Trimethoprim, Pyrimethamine, and Cycloguanil analogues using extremely randomized trees, *J. Mol. Graphics Modell.*, 71, 13–27.
- [14] Inthajak, K., Toochinda, P., and Lawtrakul, L., 2018, Application of molecular docking and PSO–SVR intelligent approaches in antimalarial activity prediction of enantiomeric cycloguanil analogues, *SAR QSAR Environ. Res.*, 29 (12), 957–974.
- [15] Yuthavong, Y., Vilaivan, T., Chareonsethakul, N., Kamchonwongpaisan, S., Sirawaraporn, W., Quarrell, R., and Lowe, G., 2000, Development of a lead inhibitor for the A16V+S108T mutant of dihydrofolate reductase from the cycloguanil-

- resistant strain (T9/94) of *Plasmodium falciparum*, *J. Med. Chem.*, 43 (14), 2738–2744.
- [16] ChemAxon, 2015, Marvin was used for drawing, displaying and characterizing chemical structures, substructures and reactions, Marvin 5.12.3, ChemAxon.
- [17] O'Boyle, N.M., Banck, M., James, C.A., Morley, C., Vandermeersch, T., and Hutchison, G.R., 2011, Open Babel: An Open chemical toolbox, *J. Cheminf.*, 3 (1), 33.
- [18] Stewart, J.J.P., 2016, *MOPAC2016*, Stewart Computational Chemistry, Colorado Spring, USA.
- [19] Tosco, P., Balle, T., and Shiri, F., 2011, Open3DALIGN: An open-source software aimed at unsupervised ligand alignment, *J. Comput.-Aided Mol. Des.*, 25 (8), 777–783.
- [20] Tosco, P., and Balle, T., 2011, Open3DQSAR: A new open-source software aimed at high-throughput chemometric analysis of molecular interaction fields, *J. Mol. Model.*, 17 (1), 201–208.
- [21] Goodford, P., 2006, "The basic principles of GRID" in *Molecular Interaction Fields: Applications in Drug Discovery and ADME Prediction*, Eds. Cruciani, G., Manhold, R., Kubinyi, H., and Folkers, G., John Wiley & Sons, Inc., Hoboken, New Jersey, United States.
- [22] Pastor, M., Cruciani, G., and Clementi, S., 1997, Smart region definition: A new way to improve the predictive ability and interpretability of three-dimensional quantitative structure-activity relationships, *J. Med. Chem.*, 40 (10), 1455–1464.
- [23] Golbraikh, A., and Tropsha, A., 2002, Beware of q^2 !, *J. Mol. Graphics Modell.*, 20 (4), 269–276.
- [24] Ojha, P.K., Mitra, I., Das, R.N., and Roy, K., 2011, Further exploring r_m^2 metrics for validation of QSPR models, *Chemom. Intell. Lab. Syst.*, 107 (1), 194–205.
- [25] Chtita, S., Aouidate, A., Belhassan, A., Ousaa, A., Taourati, A.I., Elidrissi, B., Ghamali, M., Bouachrine, M., and Lakhlifi, T., 2020, QSAR study of N-substituted oseltamivir derivatives as potent avian influenza virus H5N1 inhibitors using quantum chemical descriptors and statistical methods, *New J. Chem.*, 44 (5), 1747–1760.
- [26] Sahigara, F., Mansouri, K., Ballabio, D., Mauri, A., Consonni, V., and Todeschini, R., 2012, Comparison of different approaches to define the applicability domain of QSAR models, *Molecules*, 17 (5), 4791–4810.
- [27] DeLano, W.L., 2015, *The PyMOL Molecular Graphics System*, Version 1.8, Schrödinger, LLC.
- [28] Vanichtanankul, J., Taweechai, S., Uttamapinant, C., Chitnumsub, P., Vilaivan, T., Yuthavong, Y., and Kamchonwongpaisan, S., 2012, Combined spatial limitation around residues 16 and 108 of *Plasmodium falciparum* dihydrofolate reductase explains resistance to cycloguanil, *Antimicrob. Agents Chemother.*, 56 (7), 3928–3935.
- [29] Koes, D.R., Baumgartner, M.P., and Camacho, C.J., 2013, Lessons learned in empirical scoring with smina from the CSAR 2011 benchmarking exercise, *J. Chem. Inf. Model.*, 53 (8), 1893–1904.
- [30] Laskowski, R.A., and Swindells, M.B., 2011, {LigPlot}+: Multiple ligand-protein interaction diagrams for drug discovery, *J. Chem. Inf. Model.*, 51 (10), 2778–2786.
- [31] Abraham, M.J., Murtola, T., Schulz, R., Páll, S., Smith, J.C., Hess, B., and Lindah, E., 2015, GROMACS: High performance molecular simulations through multi-level parallelism from laptops to supercomputers, *SoftwareX*, 1-2, 19–25.
- [32] Bussi, G., Donadio, D., and Parrinello, M., 2007, Canonical sampling through velocity rescaling, *J. Chem. Phys.*, 126 (1), 014101.
- [33] Berendsen, H.J.C., Postma, J.P.M., van Gunsteren, W.F., DiNola, A., and Haak, J.R., 1984, Molecular dynamics with coupling to an external bath, *J. Chem. Phys.*, 81 (8), 3684–3690.
- [34] Agrawal, P., Singh, H., Srivastava, H.K., Singh, S., Kishore, G., and Raghava, G.P.S., 2019, Benchmarking of different molecular docking methods for protein-peptide docking, *BMC Bioinf.*, 19 (13), 426.